JOURNAL OF GEOPHYSICAL RESEARCH, VOL. 103, NO. D24, PAGES 31,955-31,968, DECEMBER 27, 1998

SCAR-B fires in the tropics: Properties and remote sensing from EOS-MODIS

Yoram J. Kaufman

Laboratory for Atmospheres, NASA Goddard Space Flight Center, Greenbelt, Maryland

Richard G. Kleidman

Science Systems and Applications, Inc., Laboratory for Atmospheres, NASA Goddard Space Flight Center, Greenbelt, Maryland

Michael D. King

Earth Sciences Directorate, NASA Goddard Space Flight Center, Greenbelt, Maryland

Abstract. Two moderate resolution imaging spectroradiometer (MODIS) instruments are planned for launch in 1999 and 2000 on the NASA Earth Observing System (EOS) AM-1 and EOS PM-1 satellites. The MODIS instrument will sense fires with designated 3.9 and 11 μm channels that saturate at high temperatures (450 and 400 K, respectively). MODIS data will be used to detect fires, to estimate the rate of emission of radiative energy from the fire, and to estimate the fraction of biomass burned in the smoldering phase. The rate of emission of radiative energy is a measure of the rate of combustion of biomass in the fires. In the Smoke, Clouds, and Radiation-Brazil (SCAR-B) experiment the NASA ER-2 aircraft flew the MODIS airborne simulator (MAS) to measure the fire thermal and mid-IR signature with a 50 m spatial resolution. These data are used to observe the thermal properties and sizes of fires in the cerrado grassland and Amazon forests of Brazil and to simulate the performance of the MODIS 1 km resolution fire observations. Although some fires saturated the MAS 3.9 μm channel, all the fires were well within the MODIS instrument saturation levels. Analysis of MAS data over different ecosystems, shows that the fire size varied from single MAS pixels (50 x 50 m) to over 1 km^2. The 1 x 1 km resolution MODIS instrument can observe only 30-40% of these fires, but the observed fires are responsible for 80 to nearly 100% of the emitted radiative energy and therefore for 80 to 100% of the rate of biomass burning in the region. The rate of emission of radiative energy from the fires correlated very well with the formation of fire burn scars (correlation coefficient = 0.97). This new remotely sensed quantity should be useful in regional estimates of biomass consumption.

1. Introduction

In the Smoke, Clouds, and Radiation-Brazil (SCAR-B) experiment, tens of thousands of fires and their emitted smoke were detected by the MODIS airborne simulator (MAS) in 50 spectral channels spanning from the visible to the thermal IR [*King et al.*, 1996]. These data are used here to characterize the fires in the Amazon forest and the cerrado grassland savannas and to assess the capability of the new spaceborne MODIS instrument, scheduled to be launched on the Earth Observing System (EOS) AM-1 satellite in early 1999, and provide daily global fire data at 1030 and 2230 local equatorial crossing time. A second MODIS will be launched on the EOS PM-1 satellite in late 2000 and will acquire global observations at 1330 and 0130 LT. MODIS is equipped with two special fire channels, at 3.9 and 11 μm, which saturate at about 450 and 400 K, respectively. The MODIS 1.6 and 2.1 μm channels are also sensitive to fires at night, but routine acquisition of these channels is not planned during the nighttime period of the satellite orbit. The 3.9 and 11 μm channels will be used to detect fires and to estimate the rate of emission of radiative energy (E_f) from the fires [*Kaufman et al.*, 1998]. E_f can be used as an indicator of the instantaneous rate of combustion of biomass in the fire [*Kaufman et al.*, 1996]. Note that E_f will be referred to in this paper also as radiative energy or fire energy, all of which refer to the same quantity of the rate of emission of radiative energy in MW from the fire. On a statistical basis the rate of combustion of biomass by fires can form an additional pathway to estimate emissions from biomass burning [*Crutzen et al.*, 1979; *Crutzen and Andreae* 1990; *Kaufman et al.*, 1990]. Current estimates are based on analysis of the population distribution and agricultural practices [*Hao et al.*, 1994]. Recently analysis of satellite data of burn scars was used to estimate the rate of biomass burning in Africa. Surprisingly, the analysis showed significantly smaller rates of grass fires than previous estimates that did not use remote sensing [*Justice et al.*, 1996]. For individual wild fires the rate of combustion is an indicator of the strength and danger of a fire and can be useful in fire fighter decisions. In order to quantitatively use the rate of emission of radiation from the fire, field and laboratory experiments are carried out to relate E_f

Paper number 98JD02460.

to the rate of consumption of biomass in the fire and to the rate of emission of trace gases and aerosol from the fire [*Kaufman et al.*, 1996]. On an experimental basis, MODIS will also be used to estimate the fraction of the radiative energy emitted in the smoldering phase. Emissions of partially oxidized organic matter in the form of trace gases and aerosol particles are higher in the smoldering than in the flaming stage [*Ward and Hardy*, 1991; *Ward et al.*, 1992, 1996a, b; *Hao et al.* , 1996; *Kaufman et al.*, 1997]; therefore an estimate of the fraction of biomass consumed in the smoldering phase can help in the estimation of emissions.

2. Radiation Measurements

The MODIS airborne simulator (MAS) is a scanning spectrometer with 50 spectral bands ranging in the wavelength from 0.55 to 14.2 μm. Flown aboard the NASA ER-2 high-altitude research aircraft, the MAS, shown in Figure 1, scans through nadir in a plane perpendicular to the velocity vector of the aircraft (cross track), with the maximum scan angle extending 43° on either side of nadir (86° full swath aperture). At a nominal ER-2 altitude of 20 km this yields a swath width of 37 km centered on the aircraft ground track. A total of 716 Earth-viewing pixels are acquired per scan at a scan rate of 6.25 Hz. Information provided by the aircraft inertial navigation system is used to adjust the timing of the digitizer, providing up to ±3.5° of roll compensation, in 0.03° increments. With each pixel having a 2.5 mrad (0.14°) instantaneous field of view, the spatial resolution at nadir is 50 m from the nominal aircraft altitude of 20 km. Table 1 summarizes the MAS specifications. A detailed description of the optical, mechanical, electronics, and data acquisition system design of the MAS can be found in the work of *King et al.* [1996].

Radiometric calibration of the shortwave (<2.5 μm) channels is obtained by observing laboratory standard integrating sphere sources on the ground before and after each deployment. The absolute calibration of the MAS is determined by viewing the output of a 30" integrating sphere (76 cm) maintained at Ames Research Center. This sphere is coated with $BaSO_4$ paint and internally illuminated by 12 quartz-halogen lamps. The highly Lambertian radiation exiting the 20 cm opening on the top of the sphere is viewed by the nadir-scanning MAS, with the output counts monitored as a function of intensity (radiance) for varying numbers of lamps turned on inside the sphere.

Since the 30" sphere does not typically travel to field deployments (and did not travel to Brazil for SCAR-B), a 20" (51 cm) hemisphere is shipped and set up beneath the MAS

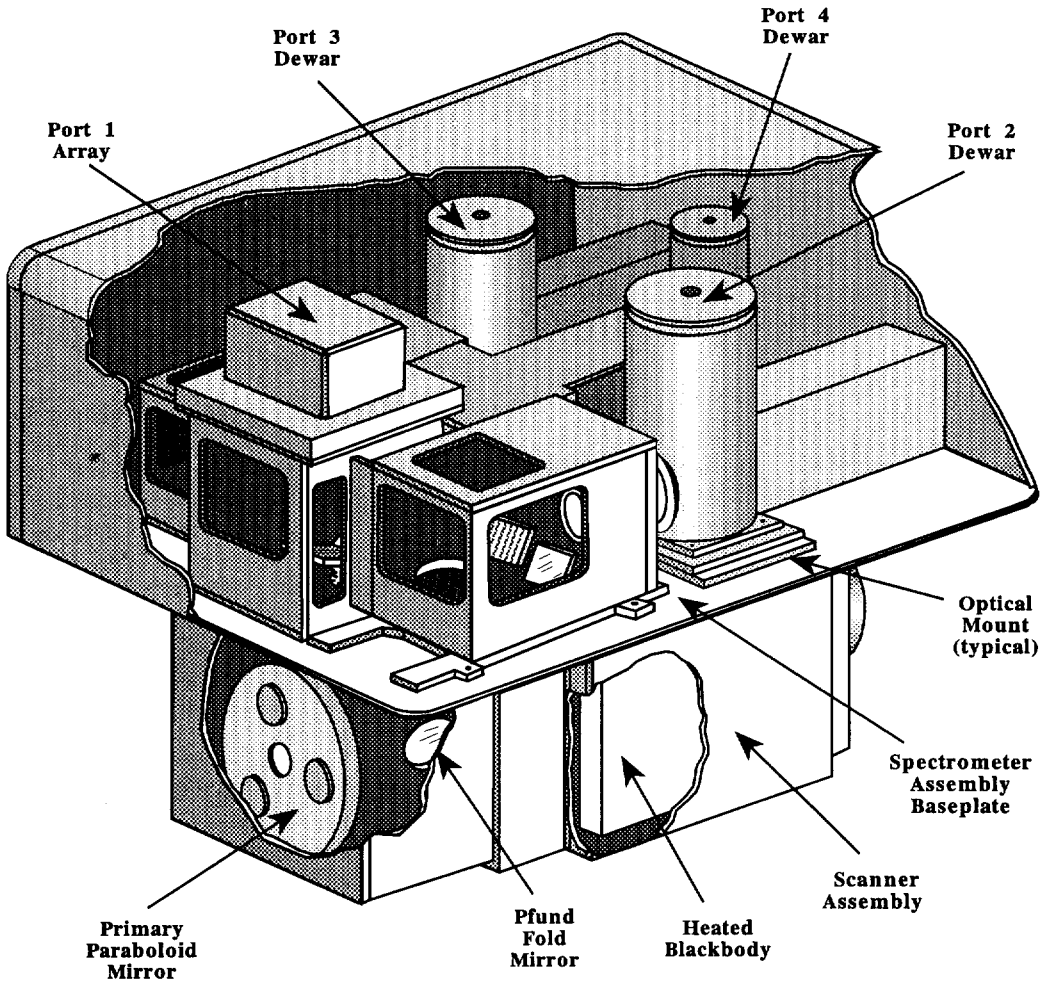

Figure 1. Cutaway drawing of the MODIS airborne simulator (MAS). The spectrometer housing and scanner subassembly are approximately 60 cm long, 46 cm wide, and 48 cm deep, with the total system weighing 96 kg.

Table 1. MODIS Airborne Simulator Specifications

Item	Specification
Platform	NASA ER-2 aircraft
Altitude	20 km (nominal)
Ground speed	206 m s^{-1} (nominal)
Total field of view	85.92°
Swath width	37.25 km (at 20 km altitude)
Instantaneous field of view	2.5 mrad
Pixel spatial resolution	50 m (at 20 km altitude)
Pixels per scan line	716 (roll corrected)
Scan rate	6.25 Hz
Spectral channels	50
Spectral range	0.55-14.2 μm
Data channels	50
Bits per channel	12; 16-bit dynamic range
Data rate	358 kb s^{-1} = 1.29 Gb h^{-1}
Visible calibration	integrating sphere on the ground
Infrared calibration	two temperature controlled blackbodies on board
Temperature sensitivity	thermal chamber and integrating sphere in laboratory
Spectral calibration	monochromator and FTIR in laboratory

FTIR, Fourier transform infrared radiometer.

prior to each ER-2 flight to monitor day-to-day variations in the MAS shortwave calibration. The 20" integrating hemisphere is coated with Duraflect™ by Labsphere and is internally illuminated by 10 lamps. Recent intercomparisons suggest that this smaller, more portable, source is suitable for MAS field calibration purposes.

Finally, prior to deployment to Brasília, the MAS was put in a thermal chamber along with the 20" integrating hemisphere as the operating temperature of the MAS was lowered. In this way, the temperature dependence of the MAS shortwave calibration was determined.

Calibration of the infrared channels is obtained by viewing two onboard blackbody sources once every scan. The blackbody sources are located on either side of the scan aperture in the scanner subassembly, with one operated at the ambient temperature of the ER-2 (typically -19°C) and the other (shown in Figure 1) operated at an elevated temperature (typically 30°C). After making allowance for the emissivity of the blackbodies (which range from 0.94 to 0.98, depending on wavelength), the longwave calibration of the MAS has been estimated to be good to within 1°C [*King et al.*, 1996].

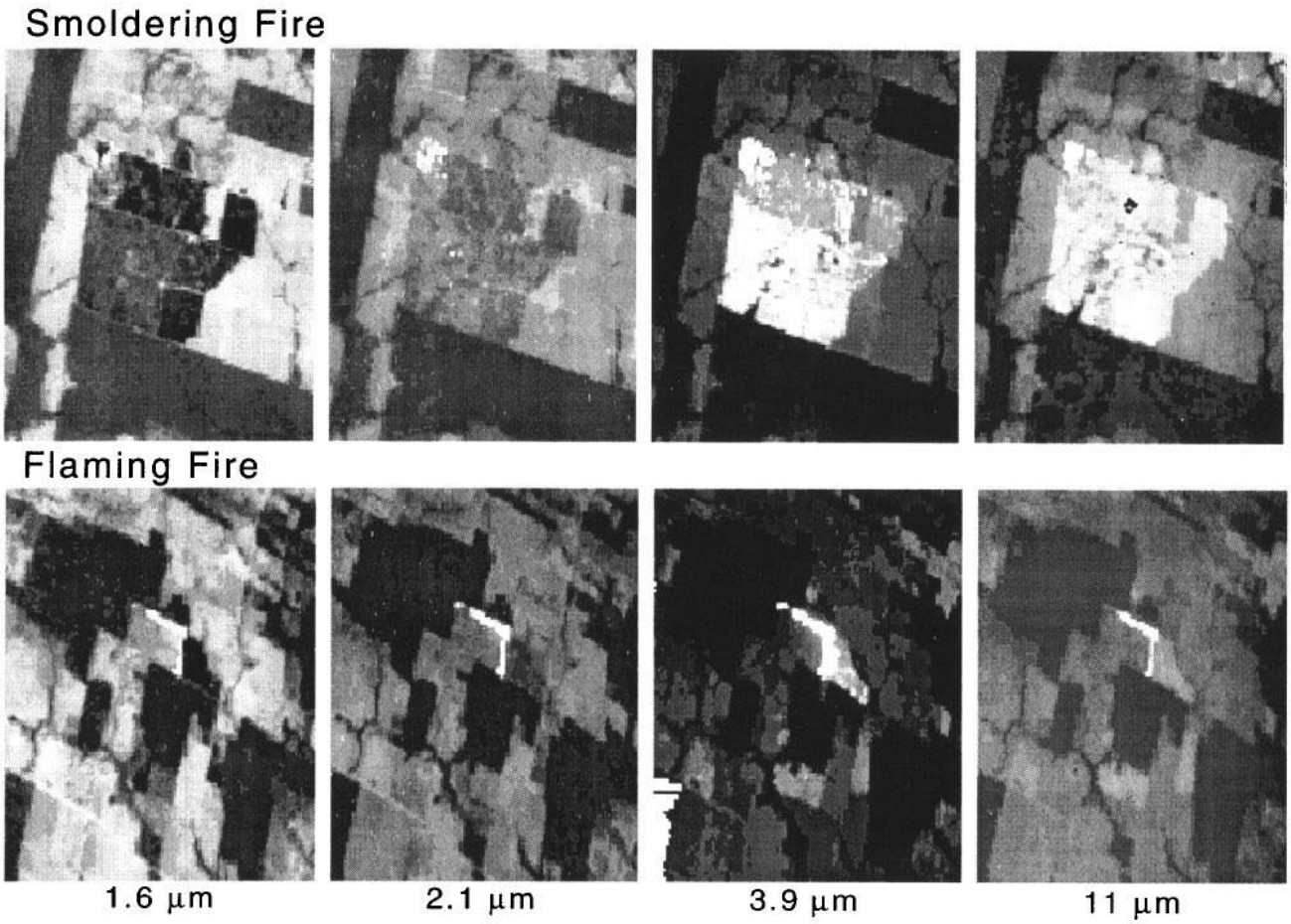

Figure 2. Example of the thermal properties of two fires observed from the MAS instrument onboard the NASA ER-2 aircraft over Alta Floresta, Brazil (10°S, 56°W): (top) large smoldering fire; (bottom) edge of a flaming fire. The fire properties are shown at 1.6, 2.1, 3.9, and 11 μm. While the 1.6 μm channel is sensitive only to the flaming zone with apparent temperatures in excess of 650 K, the longer wavelengths are sensitive to progressively lower fire temperatures and larger fire zones ($T > 520$ K for 2.1 μm; $T > 310$K for 3.9 μm; and any temperature at 11 μm). Note that the strongest contrast between the fire and its surrounding background is at 3.9 μm. Detailed information on these fires is given in Table 2.

Table 2. Summary of Properties of Two Fires in Figure 2

Parameter	Wavelength 1.6 μm	2.1 μm	3.9 μm	11 μm
	Top Fire in Figure 2 *(No. of MAS Pixels: 565, corresponding to 1.4 km^2)*			
Average temperature	339 K	454 K	336 K	310 K
Radiative energy	22 MW	29 MW	39 MW	50 MW
Ratio of smoldering energy to total ($E_{11}/E_{11}+E_{1.6}$)			*0.69*	
	Bottom Fire in Figure 2 *(No. of MAS Pixels: 120, corresponding to 0.3 km^2)*			
Average temperature	540 K	538 K	391 K	320 K
Radiative energy	113 MW	214 MW	64 MW	43 MW
Ratio of smoldering energy to total ($E_{11}/E_{11}+E_{1.6}$)			*0.28*	

MAS, MODIS airborne simulator.

3. Statistical Properties of Fires in Brazil

The MAS instrument on the ER-2 flew over 70 hours in Brazil covering 2 million km^2 with 50 channels and 50 m resolution data [*King et al.*, this issue]. Out of this data set we selected four regions in the Amazon and cerrado to demonstrate the statistical properties of the fires, their size, and thermal signature. Examples of fire observations in four spectral channels (1.6, 2.1, 3.9, and 11 μm) are shown in Figure 2. The properties of these fires are summarized in Table 2. The threshold for detecting the presence of the fire and its temperature varies from 650 K for 1.6 μm to 520 K for 2.1 μm

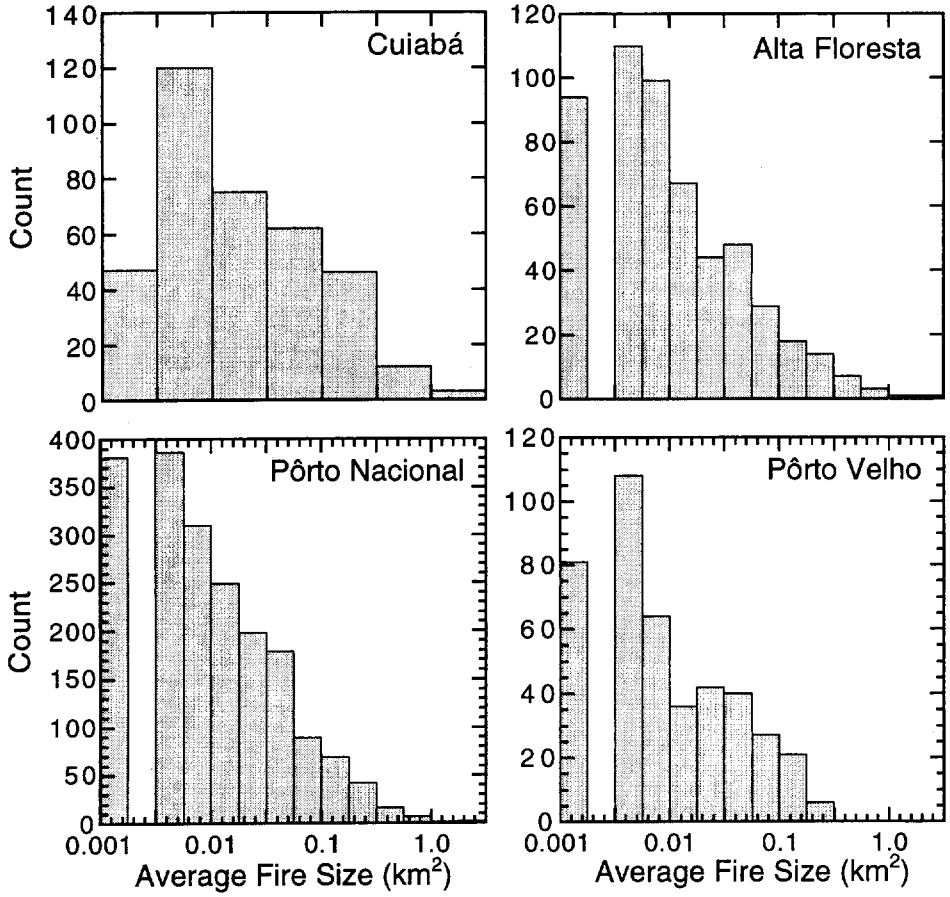

Figure 3. Statistics of fire size in Brazil obtained from MAS observations over Cuiabá in the central Brazil cerrado (agriculture and dry grass fires), north of Pôrto Nacional (dense cerrado in the northwest of Brazil), Alta Floresta on the southern edge of the Amazon Basin (mainly secondary forest fires), and Pôrto Velho on the western part of the Amazon Basin (primary forest fires). The fire size is the result of combination of 50 m resolution MAS pixels. Comparison with the 20 m resolution AVIRIS data shows that the MAS fires are 14% too large.

and to 315 K for 3.9 μm. Eleven micrometers can observe much lower temperatures, on a continued spectrum from nonfire pixel to a fire. The top fire in Figure 2 is a large, mostly smoldering fire that generates no appreciable response at 1.6 μm and only a small response at 2.1 μm. The bottom fire is a flaming front with a strong response at 1.6 μm and the other channels. The 3.9 μm channel is the most sensitive to the presence of fire, with the best contrast from the surrounding background in both cases presented in Figure 2. Therefore the size of a fire is determined from the number of MAS pixels that are detected as fires at 3.9 μm. We found empirically that an apparent temperature at 3.9 μm of 335 K does a good job of separating fires from nonfire regions. It is assumed that MAS pixels that pass this threshold are completely covered by fire. As a result, the actual fire size could be smaller. Intercomparison between 16 fires observed with the 50 m resolution MAS instrument and with the 20 m resolution AVIRIS instrument showed a correlation coefficient of 0.98 between the two measures of fire sizes. The MAS fire sizes were 16% larger than the fires detected by Airborne Visible and Infrared Imaging Spectrometer (AVIRIS) using the same 2.1 μm channels. Any MAS fire pixels less than 1 km distant from each other are grouped into a single fire.

Statistics of fire size in four ecological regions of Brazil are shown in Figure 3. These regions represent different fire types from dry cerrado with agriculture fires in Cuiabá to dense cerrado in Pôrto Nacional, dense primary deforestation fires in Pôrto Velho, and secondary burns in Alta Floresta. The fire size statistics are very similar in all four regions.

4. Analysis of the Radiative Energy Emitted From Fires

The radiative energy of fires can be derived from several channel combinations, each with different sensitivity to surface heterogeneity and emissivity. Simulations showed that the 3.9 μm channel is the best for deriving fire radiative energy since, for this channel, the relationship between the fire radiative energy and the apparent temperature is least sensitive to the mixture of temperatures in the fires [*Kaufman et al.*, 1998]. This also fits the observations in Figure 2 that at 3.9 μm the contrast between the fire and the surrounding regions is the greatest. Since the fire is not homogeneous, an empirical relationship between the radiative energy from the fire and its average apparent temperature has to be used. This relationship was derived for MODIS from simulations of hundreds of heterogeneous fires with different mixtures of smoldering and flaming combustion and different fire temperature composites [*Kaufman et al.*, 1998]. In the simulations, each pixel was composed of 100 subregions, each of which had a random fire temperature chosen from the range 600 K ± 100 K for smoldering and 1000 K ± 200 K for flaming

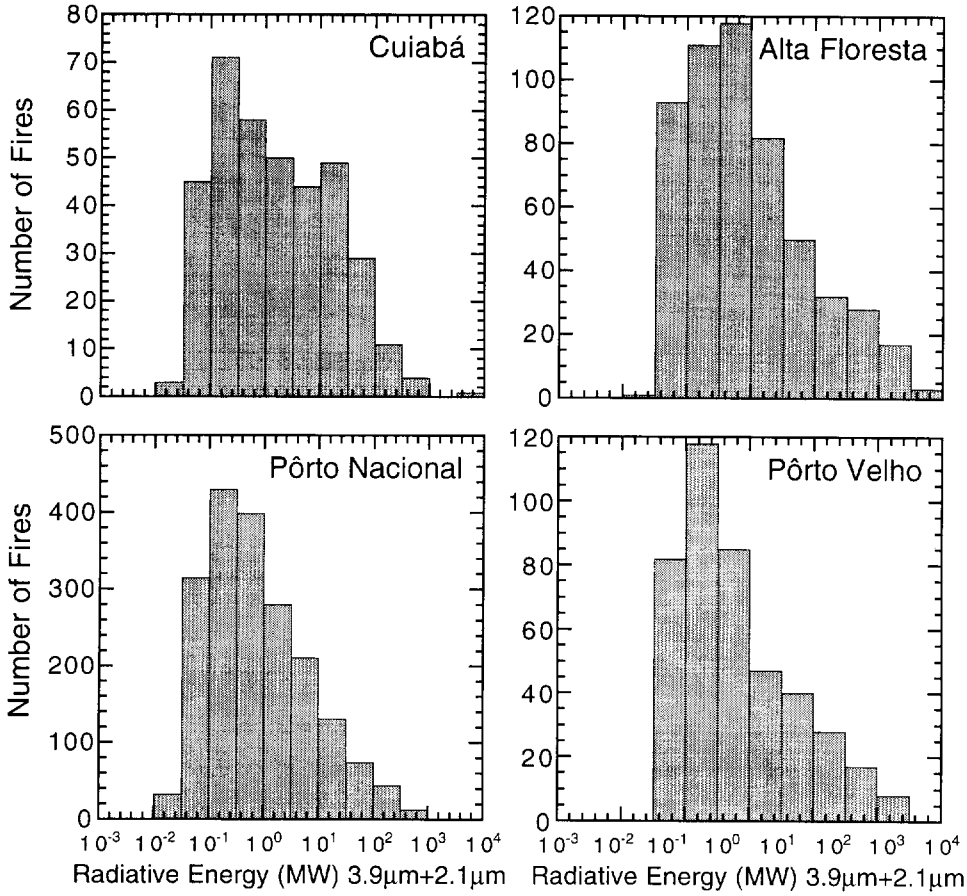

Figure 4. Statistics of the rate of emission of radiative energy from fires in Brazil derived from MAS measurements at 3.9 and 2.1 μm (equation (3)) over Cuiabá, Pôrto Nacional, Alta Floresta, and Pôrto Velho. The radiative energy is an indicator of the rate of combustion. The statistics of the radiative energy are derived from observations of the same fires used in the statistics of fire size presented in Figure 3.

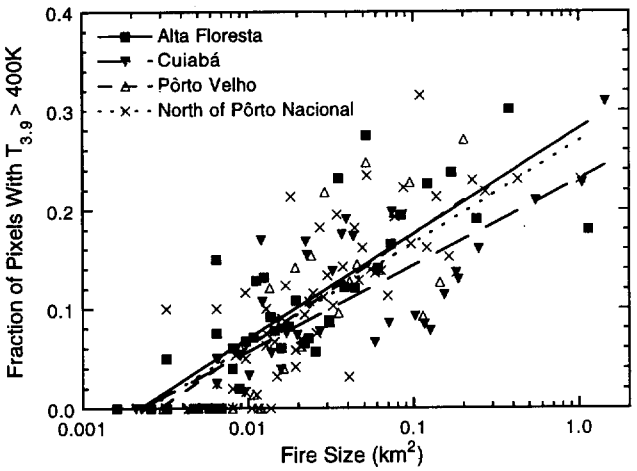

Figure 5. Fraction of the fire with MAS pixels hotter than $T_{3.9}$ > 400 K. Data are sorted as a function of the fire energy and averaged in groups of 10. Lines are the logarithmic best fits to the data. The plot shows only small differences between the different ecosystems from dry cerrado in Cuiabá to dense cerrado in Pôrto Nacional, secondary forest in Alta Floresta, and primary forest in Pôrto Velho. The logarithmic fits to the data are $f=\alpha+\beta*\log(s)$, where f is the fraction of hot pixels and s is the fire size. The plots are similar with correlation coefficients between 0.85 and 0.86, values of α between 0.23 and 0.29, and values of β between 0.09 and 0.11.

combustion. Each subregion was assumed to be homogeneous with a T^4 relationship between temperature and emitted energy. For each fire, a progressive transition from flaming to smoldering was simulated. Within an error of 20% the rate of emission of radiative energy from the fire (E_f) can be described using the following relationship:

$$E_{f3.9} = 4.34 \times 10^{-19} (T_{f3.9}{}^8 - T_{b3.9}{}^8) \quad (Wm^{-2}) \quad (1)$$

where $T_{f3.9}$ is the apparent fire temperature and $T_{b3.9}$ is the temperature of the surrounding background. Subtraction of the background apparent temperature in equation (1) also in effect subtracts the contribution of solar radiation at 3.9 μm that is reflected by the surface. This equation is based on the assumption that the surface reflectance and the temperature of the region surrounding the fire are homogeneous. This assumption will be examined later using MAS data. The calibration of the 3.9 μm channel is uncertain for high temperatures, and the channel saturates at ~ 510 K [*King et al.*, this issue]. Therefore for pixels with apparent temperatures $T_{f3.9}$ > 400 K, the radiative energy is derived from a shorter-wavelength channel at 2.1 μm using an empirical formula derived in a manner similar to equation (1).

$$E_{f2.1} = [(T_{f2.1} \cdot 300/49]^4 \quad (Wm^{-2}) \quad (2)$$

The total estimate of the rate of emission of radiative energy is therefore

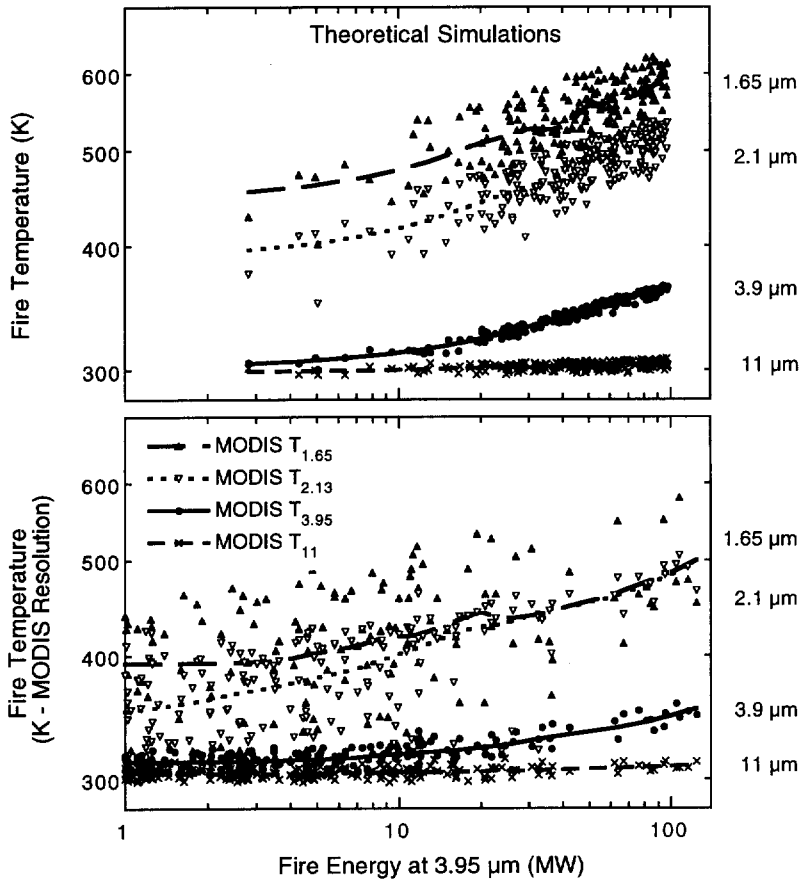

Figure 6. Comparison between theoretical (top) and measured (bottom) relationships of the fire mid-IR and IR apparent temperature in several spectral bands and the rate of emission of thermal energy (E_f) from the fire. For the MAS data, E_f is computed from the detected signal at 3.9 μm, $T_{f3.9}$, and the background to the fire, $T_{b3.9}$: $E_{f3.9}=4.34\times10^{-19}$ ($T_{f3.9}{}^8$ - $T_{f3.9}{}^8$). For the theoretical calculations the fire energy is the summation on the blackbody radiation of the individual components of the fire.

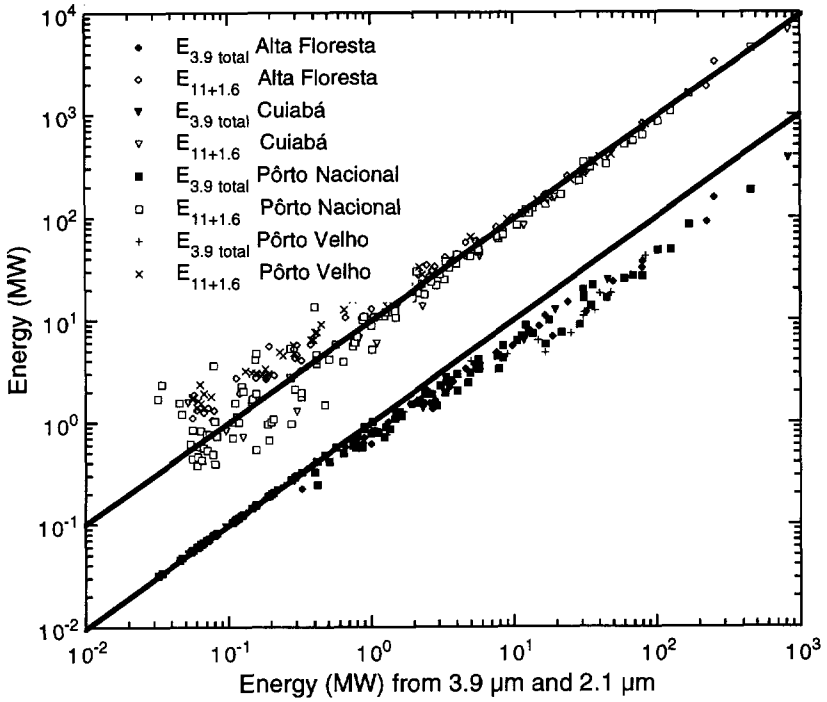

Figure 7. Relationship between the fire energy detected in three different channel combinations of MAS data. The values for 11 μm + 1.6 μm, given by the open symbols, are shifted upward by one decade for clarity. Before plotting, the data were sorted as a function of fire size and then averaged in groups of 10. The solid lines represent the lines of a perfect fit between the energy estimates. The correlation coefficients for the power law relationship between the energies at the different channel combinations were between 0.97 and 1.0.

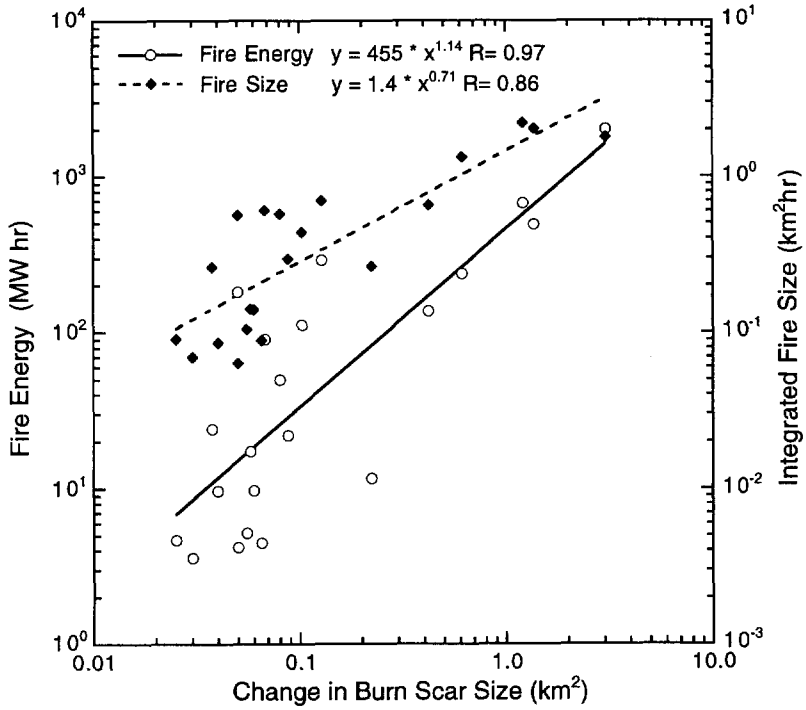

Figure 8. Integrated radiative energy emitted from the fire (left scale) and integrated fire size (right scale) as a function of the growth in the burn scar. MAS data from September 11, 1995, over a dense cerrado region north of Pôrto Nacional were used. Here every fire was observed several times by consecutive ER-2 flights. Each observation provided the fire thermal radiative energy by using a composite of the radiance at 3.9 and 2.1 μm, $E_{f3.9/2.1}$. The fire size was also determined. The ordinate shows the integral of these quantities as a function of time. The abscissa is the difference between the burn scar in the first and last flight over each fire. The power law correlation between the integrated radiative energy and the change in burn scar is 97%. The correlation between the burn scar and the integrated fire size is 86%.

$E_{f3.9/2.1} = \sum E_f$, where $E_f = \{E_{f3.9}$ for $T_{f3.9} < 400K$

$E_{f2.1}$ for $T_{f3.9} > 400K$ (W/m^{-2}) (3)

and the summations are over all the fire pixels. Later on we shall compare the use of only the 3.9 μm channel (equation (1)) and the use of the combined 3.9 and 2.1 μm channels (equation (3)).

The 11 μm channel is mostly sensitive to smoldering conditions and the 1.6 μm channel is mostly sensitive to flaming conditions. In simulations the 2.1 μm channel was found to be equally sensitive to smoldering and flaming radiative energies, but it is also sensitive to surface reflectance of sunlight and therefore can be used only for very energetic fire pixels. In addition to the use of the 3.9 μm channel alone (equation (1)) for fire energy and the combination of 3.9 and 2.1 μm (equation (3)), a combination of 1.6 μm, representing flaming conditions, and 11 μm, representing smoldering conditions, was used to derive the fire radiative energy:

$$E_{f1.6/11} = \sum \{E_{f1.6} + E_{f11}\} \quad (W/m^{-2}) \quad (4)$$

The statistics of the rate of emission of radiative energy from the fire using equation (3) is plotted in Figure 4 for the same four ecosystems shown in Figure 3. Note that the dry agricultural waste fires and grass fires in Cuiabá are more energetic than the fires in the other regions. A comparison of the thermal properties of fires in the different ecological regions for a given fire size is shown in Figure 5. Here the fire strength is given by the fraction of the fire pixels that are above $T_{f3.9}$ = 400 K. There are no significant differences between the fire strength in the different ecosystems for a given fire size.

For an insight into the fire thermal properties, MAS spectral measurements were compared with theoretical calculations of the expected response in each channel (Figure 6). In the theoretical calculations, made prior to the SCAR-B field experiment and independent of it, the MODIS pixels were subdivided into 100 subregions, each with an assigned temperature, similar to the one used in developing equation (1). The average radiance of each spectral channel was used to derive the simulated MODIS pixel temperature in that channel assuming that the pixel was a uniform blackbody. The total rate of emission of radiative energy from the pixels is calculated from the effective temperature at 3.9 μm using equation (1). Figure 6 shows a comparison between the MAS measurements and the theoretical calculations. The calculations were performed for the MODIS resolution of 1 km, and the MAS data were reduced to that resolution. The apparent temperatures in the individual channels were plotted as a function of the fire energy derived from 3.9 μm apparent temperature using equation (1). The agreement is remarkably good, considering the uncertainties, lending considerable strength to the assumptions behind the fire simulations. These assumptions include a given heterogeneous distribution of fire temperature, emissivity of 1.0, no atmospheric effect on the observed fire temperature, and good calibration over the entire dynamic range.

Additional insight into the fire spectral radiative properties can be obtained by observing the relationship between the fire radiative energy given by $E_{f3.9}$ and $E_{f1.6+11}$ as a function of $E_{f3.9+2.1}$ (Figure 7). The overall agreement between these different techniques is very good, though differences of a factor of 2 are possible for $E_{f1.6+11}$. For $E_{f3.9}$ the differences are much smaller, but a systematic underestimate increasing from 0 to 50% for strong fires is present, probably due to a nonlinearity of the channel for high signals above the calibration range. This general agreement increases our confidence in the MAS data and in our methodology for deriving radiative energy from them.

The remotely sensed rate of emission of radiative energy from the fire is based on a simple model of a uniform blackbody pixel. For this measure to be useful, we need a concrete relationship between this radiative energy and the rate of combustion or rate of emission of combustion products. A relationship between the radiative energy and the rate of emission of particulates from a prescribed fire was reported elsewhere [*Kaufman et al.*, 1996]. The agreement between the

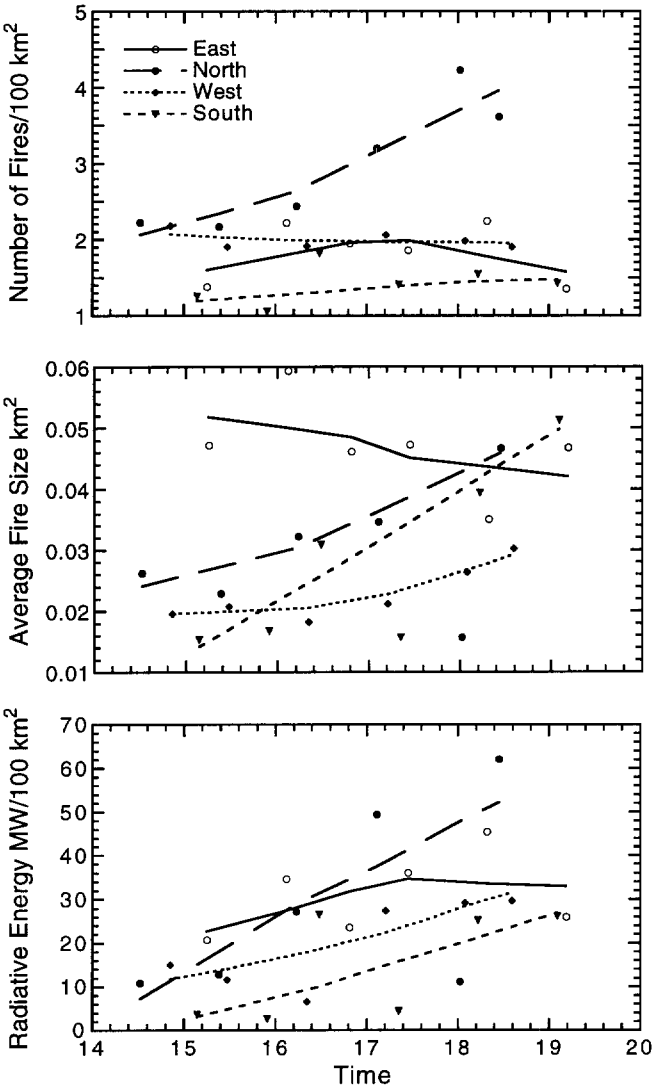

Figure 9. Time dependence of the density of fires (number of fires per 100 km²), the average size of the fire, as given by MAS 50 m resolution pixels (in kilometers squared), and rate of emission of radiative energy from the fire, derived from the 3.9 and 2.1 μm MAS channels (equation (3)). The data were obtained from six repeating ER-2 flight legs over the same box pattern bounded by the subaircraft latitude lines of 8.2°S and 9.5°S and longitude lines of 49°W and 50.5°W in a region north of Pôrto Nacional. The MAS images were 37 km wide. The average values for each of the legs of the box are given. The local time is 4 hours less than the UTC.

calculated and the measured fire spectral signal and the ability to reproduce similar fire energies using different channel combinations generates confidence in the basic physics of fire thermal radiation and their remote detection. As a first attempt, we correlate the integral of the rate of emission of radiative energy with the development of the burn scar. The best location for this application is the SCAR-B data set over an area north of Pôrto Nacional, on September 11, where the ER-2 flew a repeating ground track over the same location 6 times spaced ~45 min between each repeat flight track. The ER-2 flew a square race track pattern parallel to latitude and longitude with 80 km flight legs. The results, presented in Figure 8, show that the fire radiative energy is highly correlated (r = 97%) with the generation of the burn scar and therefore with the consumption of biomass.

The same repetitive ER-2 flight tracks were used to apply the remote sensing procedure to the time dependence of fire properties. The variation in the density of the fires (number of fires per 100 km^2), the average fire size, and the density of the total radiative energy emitted from the fires, are plotted in Figure 9. Except for the northern leg the number of fires did not increase from 1100 LT (1500 UTC) to 1500, but the density in emission of radiative energy increased due to the increase in the development and size of individual fires.

A summary of the properties of fires detected in four sites throughout Brazil and the ability of MODIS to detect some of these properties are given in Table 3. A detailed summary as a function of the fire size is given in Table 4. Similar results are obtained for the fire radiative energy detected by the two different MAS channel combinations. The fraction of the energy emitted as smoldering is much smaller for Cuiabá with grass fires and larger for Pôrto Velho and Alta Floresta with forest fires. Discussion of the expected MODIS performance above such fires is given later.

5. Thermal Properties of Nonfire Region

Fire detection depends to a large degree on the thermal properties of the region surrounding the fire. The MODIS and AVHRR satellite detection schemes use pixels of 1 km^2 resolution, much larger than most fires (see Figure 3). Because of variability of thermal properties of fires and nonfire regions, fire detection and derivation of the fire radiative energy is done by comparing the fire pixel with the surrounding region. This method assumes that the nonfire region surrounding the fire inside the satellite 1 km pixel have the same thermal properties as the surrounding region around the fire pixel [*Dozier*, 1981; *Lee and Tag*, 1990; *Kaufman et al.*, 1996]. This assumption may be in error since the probability for hot burn scars near fires can be higher than at a distance of a few kilometers from the fire. We tested this assumption using SCAR-B MAS data. In Figure 10 a comparison is made between the background characteristics at 3.9 and 11 μm at a radius of 500 m from the fire, which represents the surrounding region inside a satellite fire pixel, and the region between a radius of 500 and 5000 m, representing the satellite pixels used to estimate the background temperature. The data show a systematic difference of 1-7 K between the immediate and the removed backgrounds at 3.9 μm. The difference at 11 μm is smaller, between 0 and 3 K. The difference usually increases with an increase in fire size. Larger, well-developed fires burn longer and have more time to leave behind hot burn scars. The difference in background temperature is greater for forest fires in the Pôrto Velho region. This may be due to the presence of more woody material that retains its residual heat for longer than the more completely consumed grass and crops in Cuiabá. These differences between the background apparent temperatures are used to refine the MODIS fire detection algorithm.

Table 3. Summary of Fire Information From All locations, Based on 50 m Resolution MAS Observations and on Reduced Resolution Simulated 1 km MODIS Data

	Location			
	Cuiabá	N. of Pôrto Nacional	Alta Floresta	Pôrto Velho
	Main Type of Vegetation			
	Dry Cerrado	Dense Cerrado	Secondary Forest	Dense Forest
Parameter				
	Rate of Emission of Radiative Energy Combined From All Observed Fires (MW)			
MAS, 3.9 and 2.1 μm	10,800	23,400	7,300	3,200
MAS, 11 and 1.6 μm	8,200	16,300	5,900	2,400
MODIS 3.9 μm	11,700	26,500	8,600	4,800
Number of observed fires	365	1,929	535	425
Duration of measurements	89 min	224 min	52 min	51 min
	Fraction of Radiative Energy Emitted in Smoldering Stage			
MAS, $E_{f11}/(E_{f1.6} + E_{f11})$	0.33	0.29	0.47	0.35
MAS, $E_{f11}/E_{f3.9}$	0.25	0.21	0.37	0.26
	MODIS Detection			
Fraction of fires detected	0.32	0.32	0.40	0.42
Fraction of fire energy detected	0.99	0.81	0.96	0.94

MODIS, moderate resolution imaging spectroradiometer.

Table 4. Average Fire Energy Given by Equation (3) and Fraction of Biomass Consumed in Smoldering Stage Given by Ratio of Smoldering Energy E_{f11} and Total Energy $E_{f3.9/2.1}$ or $E_{f1.6/11}$ (Equation (4))

	Average EMAS of a Fire (MW) $E_{f3.9/2.1}$	$\frac{E_{f11}}{E_{f1.6/11}}$	$\frac{E_{f11}}{E_{f3.9/2.1}}$	Fraction of Fires Detected by MODIS	MODIS 3.9 μm Apparent Temperature, K	MODIS 11 μm Apparent Temperature, K
Alta Floresta: Total Fire Energy, 7282 MW, Fraction of Energy Detected by MODIS, 0.96						
	89	0.44	0.36	1.00	352.1	306.5
Strong	5.2	0.46	0.29	0.56	319.9	308.6
	1.4	0.83	0.51	0.32	313.2	305.0
Medium	0.5	1.0	0.37	0.21	310.8	304.5
	0.26	1.0	0.54	0.18	311.1	304.9
	0.12	1.0	0.57	0.22	311.7	305.5
Weak	0.06	1.0	0.65	0.36	312.9	306.0
Average		0.45	0.37	0.40		
Cuiabá: Total Fire Energy, 11,009 MW, Fraction of Energy Detected by MODIS, 0.99						
	189	0.32	0.25	1.0	366.6	310.5
Strong	15.4	0.38	0.22	0.65	328.0	310.1
	4.5	0.41	0.21	0.30	318.6	309.2
Medium	2.7	0.98	0.66	0.09	314.7	309.2
	0.52	1.0	0.32	0.07	313.7	309.1
	0.23	1.0	0.40	0.09	314.0	309.6
Weak	0.11	1.0	0.55	0.09	314.3	309.8
Average		0.33	0.25	0.32		
Pôrto Nacional: Total Fire Energy, 23,426 MW, Fraction of Energy Detected by MODIS, 0.81						
	78	0.29	0.21	0.84	347.2	302.0
Strong	4.8	0.31	0.15	0.36	316.4	302.1
	1.35	0.80	0.21	0.19	312.2	302.1
Medium	0.56	1.0	0.23	0.17	311.7	302.4
	0.25	1.0	0.45	0.19	311.5	302.9
	0.12	1.0	0.42	0.24	312.4	303.8
Weak	0.05	1.0	0.28	0.27	314.0	304.9
Average		0.29	0.21	0.32		
Pôrto Velho: Total Fire Energy, 3,237 MW, Fraction of Energy Detected by MODIS, 0.94						
	48.4	0.29	0.21	0.97	339.8	303.7
Strong	3.9	0.71	0.53	0.52	315.7	303.8
	0.89	1.0	0.78	0.41	316.0	305.3
Medium	0.37	1.0	0.65	0.18	311.7	303.8
	0.22	1.0	0.54	0.30	312.0	304.0
	0.11	1.0	0.63	0.26	310.8	303.4
Weak	0.05	1.0	0.85	0.31	313.0	304.6
Average		0.35	0.25	0.42		

Fraction of fires detected by MODIS, and the expected average MODIS apparent temperature at 3.9 and 11 μm are also given. The data are averaged for group of fires of a given intensity range for each of the four locations.

6. Remote Sensing of Fires From EOS-MODIS

The analysis of MAS data was used to show the size, radiative energy, and spectral properties of fires and their backgrounds in several ecosystems throughout Brazil. This information is also used to describe the ability of the 1 km resolution MODIS instrument to detect fires and derive their radiative properties. The MODIS fire algorithm includes detection of fires, computation of the rate of emission of thermal energy (which serves as a measure of the rate of combustion of biomass), and an estimation of the fraction of the fire that is in a smoldering and flaming stage. MODIS classifies pixels as having fire if their apparent temperature at 3.9 μm, $T_{3.9}$, is high; for example, $T_{3.9} > 320$ K during the day or $T_{3.9} > 315$ K at night and if the difference $\Delta T_{41} = T_{3.9} - T_{11} > 20$ K (> 10 K at night). If the pixel temperature is not too high, it may still be classified as fire if its values of $T_{3.9}$ and ΔT_{41} are higher than the background values by at least 4 standard deviations:

$$T_{3.9} > T_{3.9\,b} + 4\delta T_{3.9\,b} \quad \text{and} \quad \Delta T_{41} > \Delta T_{41b} + 4\delta\Delta T_{41b}$$

where $\delta T_{3.9\,b}$ and $\delta\Delta T_{41b}$ are the standard deviations of $T_{3.9}$ and ΔT_{41}, respectively. Because of possible differences between the background temperature inside the fire pixel and outside the pixel, the MODIS fire algorithm requires that $\delta T_{3.9\,b}$ will be at least 5 K. The fire radiative energy for MODIS is defined in the same way as for MAS using equation (1) based on thermal emission at 3.9 μm.

The MODIS fire detection confidence and fire radiative energy are plotted in Figures 11-14 as a function of cumulative radiative energy detected by MAS, for four ecosystems throughout Brazil. The apparent excess in fire temperature as detected by the MODIS 1 km pixels at 3.9 and 11 μm and the fire size are plotted. The detection confidence is defined as the

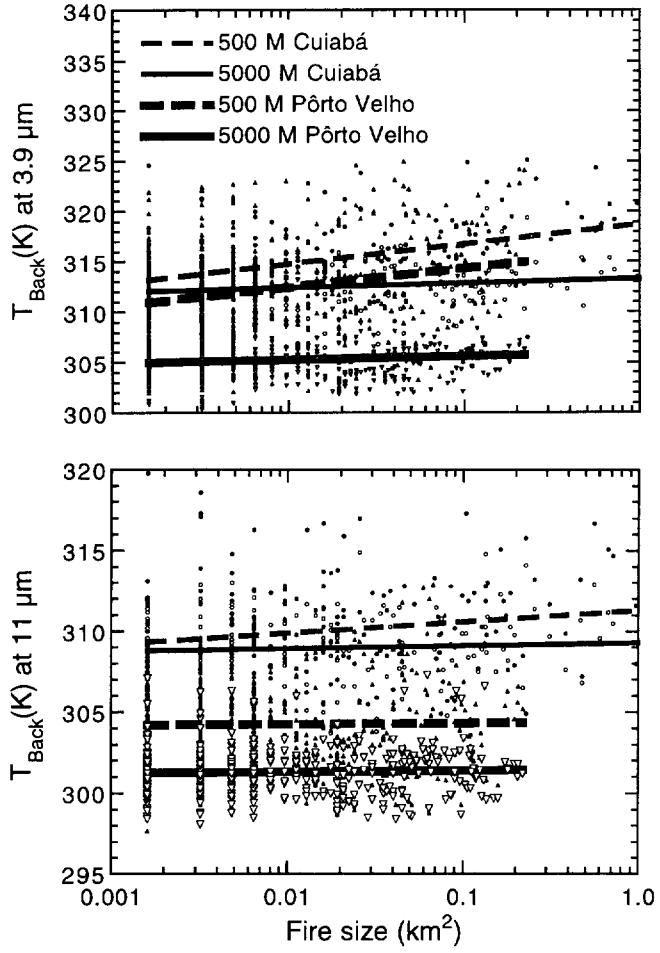

Figure 10. Apparent temperature of the background region to the fire at 3.9 and 11 μm as a function of the fire size for two background sizes: Radius of 500 and 5000 m. The 500 m radius represents the background of the fire inside the MODIS 1 km pixel and the 5000 m background represents the background outside the MODIS pixel. The dashed and solid lines are the average logarithmic fit to the data for 500 and 5000 m, respectively. Data are presented for Cuiabá with dry savanna grass and agriculture fires (black symbols and lines) and for Pôrto Velho (open symbols and lines) with dense forest fires. A systematic difference is found between the two backgrounds mainly for the Pôrto Velho region.

average detection value in all the detection criteria (the detection criteria are described in detail by *Kaufman et al.* [1998]). These figures show that even though more than half of the fires cannot be detected by MODIS (under the detection limit line in the top panels of these figures), the fires that are detected represent the 30-40% most energetic fires with cumulative energy of 80-100% (see Table 4). Because of differences between the background properties inside and outside of the 1 km resolution MODIS pixel, the actual fire energy detected by MODIS may be even larger (Table 3). Therefore these fires are responsible for most of the rate of combustion of biomass. The MODIS-detected apparent temperature at 3.9 μm is a very good measure of fire size, above a given threshold of 0.02 km² as measured by the MAS 50 m pixels. Note that in computation of the MODIS-detected radiative energy, only fires that are detected are being accounted for. The MODIS apparent temperature at 11 μm shows a significant response only for the most energetic fires. Therefore the use of information in the 11 μm channel to distinguish between smoldering and flaming fires is difficult for most fires in the tropics.

7. Partitioning Between Smoldering and Flaming

The fire apparent temperature in a given spectral channel is differently sensitive to the distribution of temperatures in the fire. The shorter the wavelength the stronger the sensitivity to higher temperatures. Therefore if the fire temperature is higher in the flaming stage than in the smoldering stage, using the apparent temperature in several spectral bands can be used to distinguish between stages of burning [*Kaufman et al.*, 1998]. The wider the spectral range the better the partitioning between smoldering and flaming can be estimated. In Figure 15

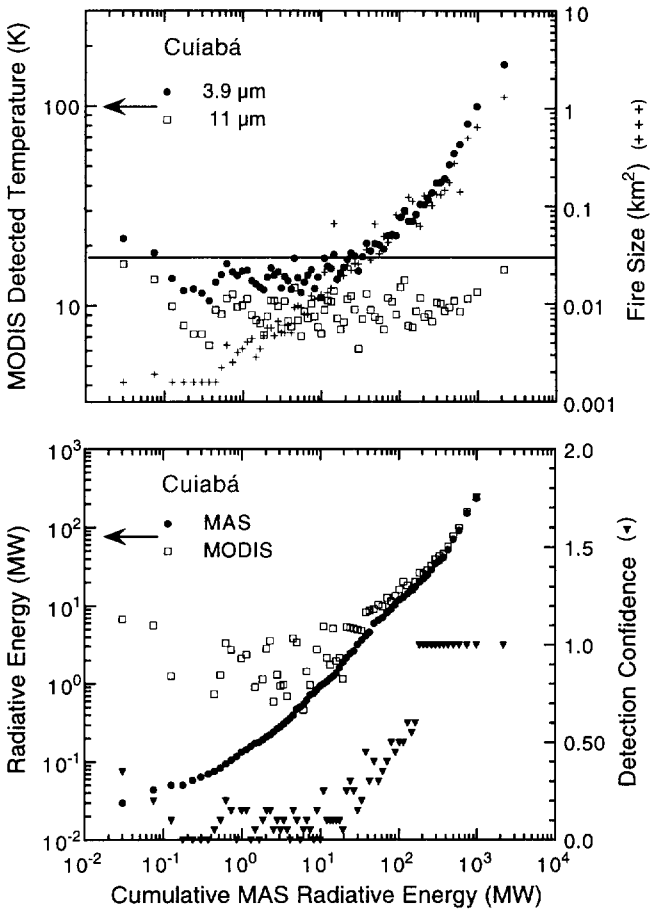

Figure 11. (top) MODIS 1 km resolution excess fire temperatures at 3.9 and 11 μm (300 K was subtracted from the apparent temperature in these channels) and fire size plotted as a function of cumulative fire energy. The fire size is based on the number of MAS 50 m pixels identified as fires. (bottom) Radiative energy detected by MAS or MODIS and the confidence of detection plotted as a function of cumulative fire energy. The data were first sorted as a function of MAS radiative energy and averaged in groups of 5. Results are presented for Cuiabá with dry cerrado and agriculture fires. The black horizontal line in the top figure corresponds roughly to the MODIS fire detection limit.

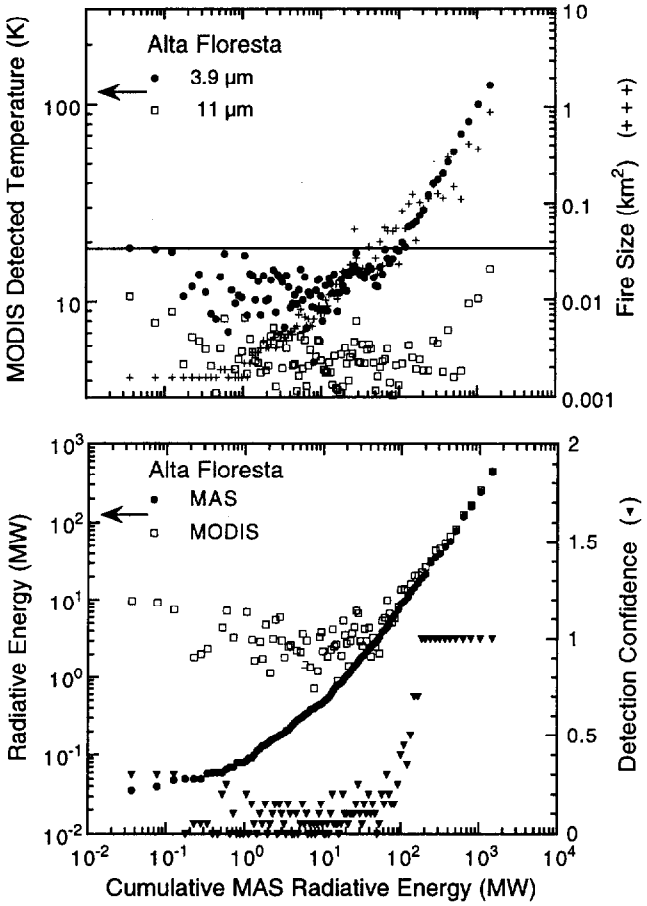

Figure 12. Same as Figure 11 but for the Alta Floresta region with forest fires.

the fraction of radiative energy in the smoldering phase is plotted as a function of time for MAS and simulated MODIS observations. For MODIS the smoldering energy is given by the radiative energy at 11 μm and the total energy by 3.9 μm, enhanced by the 2.1 μm energy for pixels with $T_{3.9} > 400$ K. For MAS, smoldering is also given by 11 μm but flaming by emission at 1.6 μm. Except for the eastern-most section of the flights on September 11, there is good agreement between the smoldering fraction derived from MAS and the MODIS channel combinations. The fraction of energy in the smoldering stage increases from 40-60% at 1100 (1500 UTC) to 50-100% at 1500 (1900 UTC). *Ward et al.* [1996b] measured a similar ratio of 55% at 1200 to 1300, but 24% at 3-4 pm, substantially lower than the present finding. Ward's measurements were in a particular location in the Pôrto Nacional area that may or may not represent the MAS observations. Therefore the ability to derive the smoldering fraction of radiative energy is still inconclusive.

8. Conclusions

The MAS data collected in Brazil during the SCAR-B experiment represents a unique data set of over 2 million square kilometer of high-resolution (50 m) fire and nonfire surface thermal properties. We used a representative part of this data set to observe fire properties in four ecosystems in Brazil and use them to foresee the performance of the MODIS spaceborne instrument that is planned to be launched on two Earth Observing System satellites. The results show that even though MODIS will not be able to observe more than half of the fires in Brazil, because of their small size and rate of burning, it will see the stronger fires that are responsible for almost all of biomass burning. The MODIS detection scheme of fires is aided by the present finding which provides basic information on the thermal properties of fires and the surrounding area not measured previously. MODIS fire channels at 3.9 and 11 μm will be used to detect the instantaneous rate of emission of radiative energy from fires. Since this measurement has not been made before from space, its detailed evaluation is needed. The good agreement between theoretical simulations of the spectral radiation from fires and the measurements from MAS reported here increases our confidence that the MODIS-measured radiative energy is representative of the rate of biomass burning. The high correlation between the integral of the rate of emission of radiative energy and the development of burn scars (r = 97%) shows that the radiative energy should be a good measure of the rate of consumption of biomass. Even so, a more detailed analysis of field and laboratory experiments is required to relate the fire radiative energy to the emission of pollution products, before we can confirm this expectation. MODIS spectral observation of fires can be used to derive the ratio between the rate of burning in the flaming and smoldering

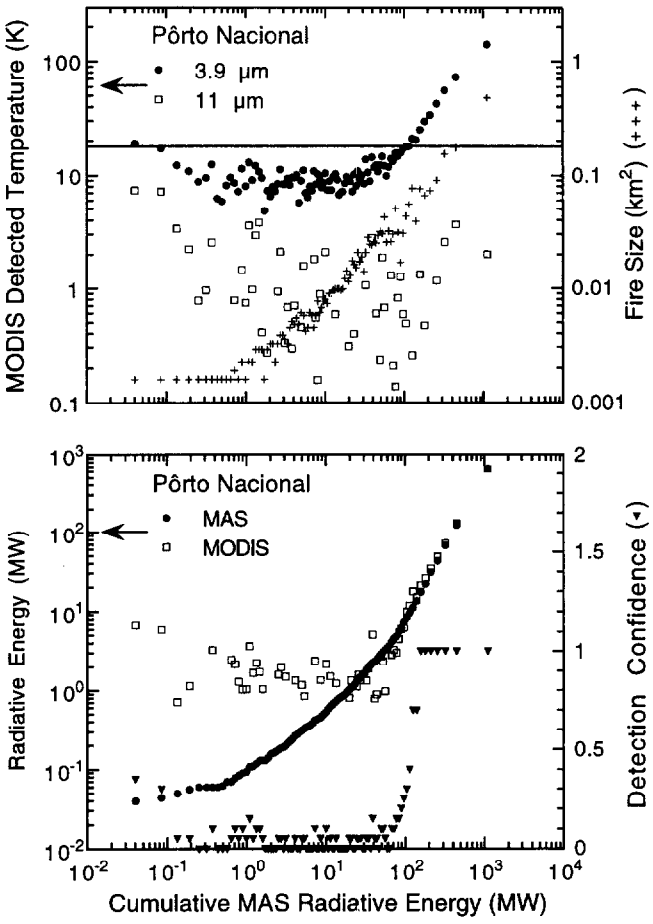

Figure 13. Same as Figure 11 but for the Pôrto Nacional region with denser cerrado.

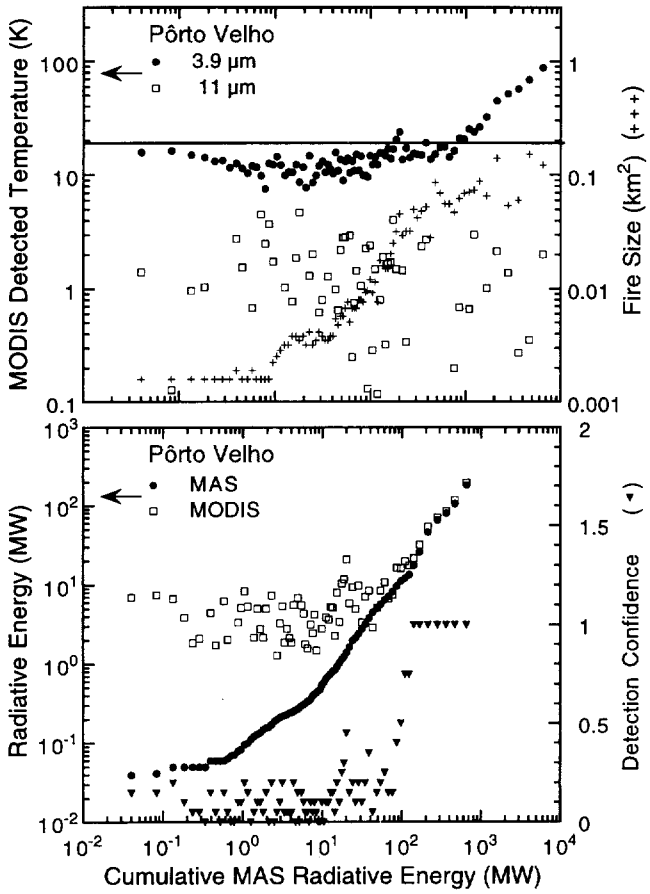

Figure 14. Same as Figure 11 but for the Pôrto Velho region with forest fires.

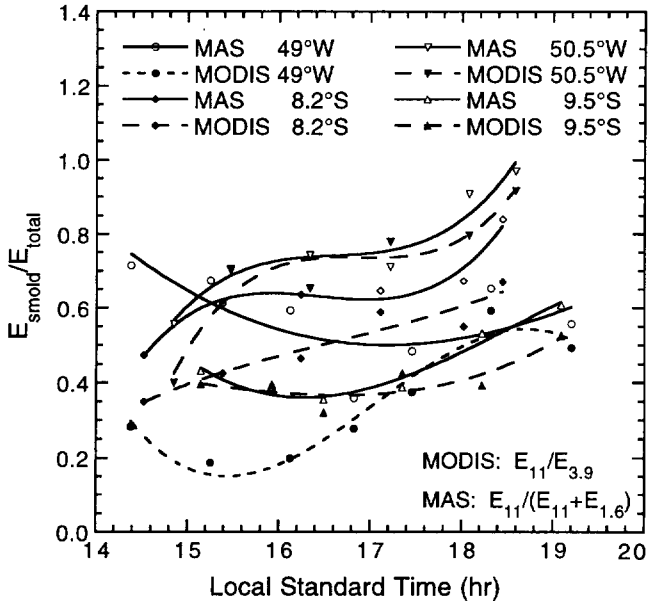

Figure 15. Comparison between the time dependence of the fraction of the radiative energy emitted in the smoldering stage as derived from MAS using 11 μm channel for the smoldering energy and the 1.6 μm channel for the flaming energy. The results are compared with the fraction of energy in the smoldering stage derived from the reduced resolution MODIS data, using 11 μm for smoldering and 3.9 μm for the total energy. The data were collected September 11, 1995, from the region north of Pôrto Nacional.

phases. However, during the day the use of only the 3.9 and 11 μm channels makes this analysis very uncertain since the partitioning between smoldering and flaming energy between 3.9 and 11 μm is not very strong and 11 μm is sensitive only to the very strong fires. The use at night of the 1.6 μm channel can enhance this partitioning significantly.

Acknowledgments. The research reported in this article was supported by the MODIS Science Team, the EOS Project Science Office, and the NASA Radiation Science Program. We are thankful to our Brazilian colleagues from INPE, IBAMA, and the University of São Paulo for their help in conducting the SCAR-B experiment and in facilitating the ER-2 flight. We are thankful to the Brazilian government for allowing the ER-2 operations in Brazil and for facilitating the logistical arrangements. The detailed review by W.-M. Hao is greatly appreciated.

References

Crutzen, P. J., and M. O. Andreae, Biomass burning in the tropics: Impact on atmospheric chemistry and biogeochemical cycles, *Science, 250*, 1669-1678, 1990.

Crutzen, P. J., L. E. Heidt, J. P. Krasnec, W. H. Pollock, and W. Seiler, Biomass burning as a source of atmospheric gases: CO, H_2, N_2O, NO, CH_3Cl, and COS, *Nature, 282*, 253-256, 1979.

Dozier, J., A method for satellite identification of surface temperature fields of subpixel resolution, *Remote Sens. Environ. 11*, 221-229, 1981.

Hao, W. M., and M.H. Liu, Spatial and temporal distribution of tropical biomass burning, *Global Biogeochem. Cycles, 8*, 495-503, 1994.

Hao, W. M., D. Ward, G. Olbu, and S. P. Baker, Emissions of CO_2, CO, and hydrocarbons from fires in diverse African savanna ecosystems, *J. Geophys. Res., 101*, 23,577-23584, 1996.

Justice C. O., J. D. Kendall, P. R. Dowty, and R. J. Scholes, Satellite remote sensing of fires during the SAFARI campaign using NOAA advanced very high resolution radiometer data, *J. Geophys. Res. , 101*, 23,851-23, 863, 1996.

Kaufman, Y. J., C. J. Tucker, and I. Fung, Remote sensing of biomass burning in the tropics, *J. Geophys. Res., 95*, 9927-9939, 1990.

Kaufman, Y. J., L. A. Remer, R. D. Ottmar, D. E. Ward, R. R. Li, R. Kleidman, R. S. Fraser, L. Flynn, D. McDougal, and G. Shelton, Relationship between remotely sensed fire intensity and rate of emission of smoke: SCAR-C experiment, in *Global Biomass Burning*, edited by J. Levin, pp. 685-696, The MIT Press, Cambridge Mass., 1996.

Kaufman, Y. J., et al., Potential global fires monitoring from EOS-MODIS, *J. Geophys. Res.*, in press, 1998.

King, M. D., et al., Airborne scanning spectrometer for remote sensing of cloud, aerosol, water vapor and surface properties, *J. Atmos. Oceanic Technol., 13*, 777–794, 1996.

King, M. D., S. C. Tsay, S. A. Ackerman, and N. F. Larsen, Discriminating heavy aerosol, clouds, and fires during SCAR-B: Application of airborne multispectral MAS data, *J. Geophys. Res.*, this issue.

Lee, T. F., and P. M. Tag, Improved detection of hotspots using the AVHRR 3.7-μm channel, *Bull. Am. Meteorol. Soc., 71*, 1722-1730, 1990.

Ward, D. E., and C. C. Hardy, Smoke emissions from wildland fires, *Environ. Int., 17,18*, 1991.

Ward, D. E., R. Susott, J. Kauffman, R. Babbitt, B. N. Holben, Y. J. Kaufman, A. Setzer, R. Rasmussen, D. Cumming, and B. Dias, Emissions and burning characteristics of biomass fires for cerrado and tropical forest regions of Brazil: BASE-B experiment, *J. Geophys. Res., 97*, 14,601-14,619, 1992.

Ward, D. E., W. M. Hao, R. A. Susott, R. Babbitt, R. W. Shea, J. B. Kauffman, and C. O. Justice, Effect of fuel composition on combustion efficiency and emission factors for African savanna ecosystems, *J. Geophys. Res., 101*, 23,569-23,576, 1996a.

Ward D. E., M. A. Yamasoe, Y. J. Kaufman, A. W. Setzer, E. M. Prins, R. E. Babbitt, R. A. Susott, and W. M. Hao, A technique for validating emission production models test results for the central region of Brazil, in SCAR-B Proceedings, 205-208, edited by V. W. J. H Kirchhoff, São Paulo, Brazil, 1996b.

Y. J. Kaufman, Laboratory for Atmospheres, NASA Goddard Space Flight Center, Code 913, Greenbelt, MD 20771. (email: kaufman@climate. gsfc.nasa.gov.)

M. D. King, Earth Sciences Directorate, NASA Goddard Space Flight Center, Greenbelt, MD 20771.

R. G. Kleidman, Science Systems and Applications, Inc., Laboratory for Atmospheres, NASA Goddard Space Flight Center, Greenbelt, MD 20771.

(Received October 1, 1997; revised June 30, 1998; accepted July 20, 1998.)